Published in final edited form as:
Traffic. 2012 October ; 13(10): 1315–1325. doi:10.1111/j.1600-0854.2012.01396.x.

Do GGA adaptors bind internal DXXLL motifs?

Balraj Doray[1], **Saurav Misra**[2], **Yi Qian**[1], **Tom J. Brett**[1,3,4], and **Stuart Kornfeld**[1,*]

[1]Department of Internal Medicine, Washington University School of Medicine, St. Louis, MO 63110

[2]Department of Molecular Cardiology, Lerner Research Institute, The Cleveland Clinic, Cleveland, OH 44195

[3]Department of Cell Biology and Physiology, Washington University School of Medicine, St. Louis, MO 63110

[4]Department of Biochemistry and Molecular Biophysics, Washington University School of Medicine, St. Louis, MO 63110

Abstract

The GGA family of clathrin adaptor proteins mediate the intracellular trafficking of transmembrane proteins by interacting with DXXLL-type sorting signals on the latter. These signals were originally identified at the carboxy-termini of the transmembrane cargo proteins. Subsequent studies, however, showed that internal DXXLL sorting motifs occur within the Nor C-terminal cytoplasmic domains of cargo molecules. The GGAs themselves also contain internal DXXLL motifs that serve to auto-regulate GGA function. A recent study challenged the notion that internal DXXLL signals are competent for binding to GGAs. Since the question of whether GGA adaptors interact with internal DXXLL motifs is fundamental to the identification of *bona fide* GGA cargo, and to an accurate understanding of GGA regulation within cells, we have extended our previous findings. We now present additional evidence confirming that GGAs do interact with internal DXXLL motifs. We also summarize the recent reports from other labs documenting internal GGA binding motifs.

Keywords

GGA proteins; DXXLL motifs; GGA cargo molecules

Introduction

The GGAs (Golgi-localized, γ-ear-containing, Arf-binding) are a family of monomeric clathrin adaptor proteins that function in receptor trafficking between the *trans*-Golgi network (TGN) and endosomes (1, 2). GGAs contain three independently folded domains. The N-terminal VHS (Vps27, Hrs, Stam) domain binds to acidic cluster-dileucine signals conforming to a DXXLL (X= any amino acid) motif. Such motifs are present in the cytoplasmic tails of cargo receptors and other integral membrane proteins that interact with GGAs. The GAT (GGA and TOM) domain interacts with the GTP-bound form of the small GTPase ARF1 and also with ubiquitin. The C-terminal GAE (γ-adaptin ear) domain binds to an array of clathrin coat accessory proteins (1, 2). In addition to these globular domains, GGAs contain an extended flexible hinge region connecting the GAT and GAE domains, through which they bind clathrin (3, 4). The consensus DXXLL motifs that interact with the

*Corresponding author: Stuart Kornfeld; skornfel@dom.wustl.edu.

GGAs are usually situated one or two residues from the carboxy (C)-terminus of the interacting membrane protein (2, 5). However, we identified an internal DXXLL motif within the hinge regions of human GGAs 1 and 3 but not GGA2. We postulated that this internal motif serves as an autoinhibitory signal that regulates the interaction of GGAs 1 and 3 with receptor tails (6). Subsequent studies from our laboratory and others identified a number of other proteins containing internal DXXLL motifs that bind GGAs (see Figure 1) (7–12).

The ability of GGAs to bind internal DXXLL motifs has recently been called into question (13). Based on structural analysis of complexes between DXXLL-motif-containing peptides and the GGA1-VHS domain, yeast two-hybrid analysis, isothermal titration calorimetry (ITC), and pull-down experiments, Cramer *et al.* did not detect binding of internal DXXLL motifs to GGA1. These investigators suggest that only C-terminal DXXLL motifs constitute active GGA-binding sites, discounting a functionally significant role for internal GGA-binding motifs in the autoinhibition of GGAs 1 and 3, and for internal GGA-binding motifs in general (13). Cramer *et al.* further posit that functional DXXLL sites must be located no more than 1-3 residues from the C-terminus of cargo proteins.

The issue of whether or not GGAs are capable of binding to internal DXXLL motifs is mechanistically important for autoinhibition, and is also significant for identification of additional cargo proteins that bind to GGAs. We have therefore extended our previous studies investigating the interaction between GGAs and internal DXXLL motifs. We now present our data confirming that GGAs bind internal DXXLL motifs, and show that this binding is modulated by amino acid residues surrounding the key aspartate and dileucines of the signal. In addition, we place our results in the context of recent reports from other laboratories documenting the presence of internal GGA-binding DXXLL motifs.

Results

Detection of GGA2 binding to the internal DXXLL motif of the LRP9 cytoplasmic tail using bio-layer interferometry

We previously characterized the interaction of GGA2 with the internal DXXLL motifs of low density lipoprotein receptor-related protein (LRP)9 and LRP12 using GST pull-down assays (9). These assays involved multiple washing steps and did not allow accurate calculation of binding affinities. We therefore confirmed the *in vitro* interaction between the internal DXXLL motif of LRP9 and GGA2 by monitoring binding in real-time using bio-layer interferometry (BLI). Purified Flag-tagged mouse GGA2 was immobilized on the BLI sensor and incubated with purified maltose-binding protein (MBP) fused to peptide sequences encoding both the internal (pLL) and C-terminal (dLL) DXXLL motifs of LRP9 (the protein encoding both motifs from hereon referred to as pLL/dLL), only the internal motif (pLL/dLL→AA), or both leucine pairs mutated to alanines (pLL→AA/dLL→AA). We utilized MBP-rather than GST-fusion peptides to avoid avidity effects from GST dimerization. Sensograms of MBP-LRP9 DXXLL peptide binding to Flag-GGA2 were recorded and used to calculate the apparent association constants after subtraction for MBP. The values were compared to those obtained with MBP fused to the C-terminal DXXLL motif of the cation-independent mannose 6-phosphate receptor (CI-MPR), a well-characterized ligand for GGAs.

As shown in Figure 2, the MBP-LRP9 30mer containing both DXXLL motifs (pLL/dLL) bound to the immobilized GGA2 in a manner similar to MBP-CI-MPR, as did the fusion protein with the C-terminal DXXLL motif mutated to AXXAA (pLL/dLL→AA). Mutation of both the internal and C-terminal DXXLL motifs (pLL→AA/dLL→AA) reduced binding to the background level seen with MBP alone. Based on these data (Table 1), we calculated

dissociation constants (K_d) of 0.12±0.04 μM, 0.15±0.04 μM, and 0.28±0.08 μM, repectively, for the CI-MPR, pLL/dLL, and pLL/dLL→AA constructs on the basis of 3 to 4 independent determinations. The absolute values for the dissociation constants determined by BLI analysis differ from published results from ITC measurements by a factor of 50. For example, we measured an affinity of 0.12 μM for CI-MPR using BLI, compared to 7.1 μM using ITC (14). It has been reported that K_d values for GGA-VHS domain/DXXLL peptide interactions measured by ITC differed from surface plasmon resonance analysis by a factor of 150–500 (15). Most importantly, however, these results confirm previous findings based on GST pull-down assays and coimmunoprecipitation experiments (8, 9). Cramer *et al.* (13) reported that deletion of the C-terminal DXXLL domain of LRP9 abolishes binding to the VHS domain of GGA1, as determined by a yeast two-hybrid assay and ITC. The reason for this striking discrepancy is unclear at this time.

Structural modeling of LRP9 and LRP12 internal DXXLL peptide interactions with the GGA1and GGA2 VHS domains

As part of their study, Cramer *et al.* used ITC to investigate binding of the GGA1 VHS domain to DXXLL motifs with and without C-terminal extensions (13). They found that a peptide encoding the GGA1 hinge sequence DDELM (Figure 1) bound to the VHS domain as tightly as a sortilin C-terminal DXXLL peptide. This was the case as long as the former terminated with two amino acids C-terminal to the LM pair; however, additional C-terminal residues beyond two resulted in loss of binding. The authors suggested that “a larger downstream segment would require a significant displacement of the loops between α6 and α7 of the VHS domain, or a sharp bend in the peptide, both of which are unlikely”. Interestingly, the LRP9 and LRP12 internal AC-LL signals ^{686}EDEDDVLLLPLAE^{698} and ^{748}EDDDDVEMLIPVSD^{761}, respectively, have downstream proline residues that could facilitate a turn in the peptide. To investigate whether such internal peptide sequences can be accommodated in the previously defined peptide binding site of GGA VHS domains, we docked corresponding peptide models into the crystal structure of the GGA1-VHS domain (16) and GGA2-VHS domain (17) using FlexPepDock (18, 19). The docking was based on co-crystal structures of C-terminal DXXLL motif peptides from CI-MPR with the VHS domain of GGA1 or GGA3 (14, 15). Only a small number of restraints were explicitly included: 1) the canonical hydrogen bonds between two VHS backbone amide groups (from F88 and R89) with the aspartic acid side-chain of the DXXLL motif; 2) the hydrogen bonds between the sidechain of a conserved asparagine (GGA1 N92) to the backbone carbonyl preceding the first leucine and the amide of the second leucine respectively. These interactions position the aspartic acid and leucines of the DXXLL motif and are conserved in GGA-VHS:peptide complexes that have been structurally characterized. As the LRP9 sequence effectively contains two overlapping internal DXXLL motifs (separated by one residue; see Figure 1), we docked the LRP9 peptide in two orientations to both GGA1-VHS and GGA2-VHS domains.

The lowest-energy models from docking show substantial agreement and preserve the appropriate orientations of the acidic and leucine sidechains from the DXXLL motifs, as expected (Figure 3, A–E). We note that both “registers” of the LRP9 peptide are accommodated by both the GGA1 and GGA2 VHS domains. Moreover, the VHS domains readily accommodate 4-5 residues following the dileucine motif with no steric clashes, deformation of the VHS domain or unusual sidechain rotamers. The peptide backbone traces a path between two clusters of sidechains near the C-termini of helices 6 and 8 of the VHS domains without clashing with residues on either helix. Our models suggest that productive hydrogen bonds and hydrophobic sidechain-sidechain interactions may further stabilize the binding of residues at the second and third position beyond the dileucine motif. For example, the residues that are located 2 positions to the C-terminus of the dileucine motif

(LRP9 P695 or L696; LRP12 P758) protrude into the groove between VHS helices 6 and 8, and make hydrophobic contacts with residues at the base of this groove. The residues located 3 positions to the C-terminus of the dileucine motif interact with S99 and K101 and pack against the aliphatic portion of the K101 sidechain in GGA1. Similarly, the residues located 3 and 4 positions to the C-terminus of the dileucine motif pack against aliphatic portions of P116 and K117 in GGA2; additional C-terminal residues may make productive contacts with the α6- α7 loop, which is more extended in GGA2 than in GGA1 (17). Finally, the lowest-energy models of the peptides show a number of salt-bridges between acidic residues preceding the canonical aspartic acid of the DXXLL motif and basic sidechains of the VHS domains, although a maximal number of salt bridges is only formed if the peptide makes a tight turn at this location.

Based on the structural modeling, we tested the effect of mutations in the residues surrounding the internal DXXLL motif of LRP12 on binding to the GGA2 VHS domain. These mutations were made in a construct encoding full-length LRP12 with the C-terminal DDEALLLC mutated to DAEAAALC. A hemagglutinin (HA) epitope was inserted in the cytoplasmic tail at E620 to facilitate detection of the protein. HA-tagged wild-type (wt) and mutant LRP12 proteins were expressed in HEK 293 cells and cell lysates were used in GST pull-down assays to measure binding to the VHS domain of GGA2. LRP12 with the C-terminal DXXLL mutations (dLL→AA) bound GGA2 as strongly as the wt protein, whereas mutation of the internal DXXLL motif in addition to the C-terminal motif (dLL→AA, pML→AA) resulted in a total loss of binding (Figure 4A). This finding agrees with results from the BLI binding assay as well as a previous pull-down study from our group that used LRP12 with a HA epitope inserted downstream of the signal sequence (9). Importantly, a P758A mutation (at the +6 position, see Figure 1) greatly impaired binding whereas a S760I mutation (at the +8 position) had no effect (Figure 4B). This result is in agreement with the model of LRP12 bound to GGA1-VHS (Figure 3C), in which P758 protrudes into the VHS domain peptide binding groove. We also examined the effects of mutations of the upstream acidic residues, E748/D749 and D750/D751, on binding of HA-LRP12 to GGA2. We found that mutation of the two residues immediately upstream of the internal DXXLL sequence in the −2/−1 positions (D750A/D751A) severely reduced binding whereas mutation of the residues in the −4/−3 positions (E748A/D749A) had a milder effect on binding (Figure 3C). The importance of acidic residues in the −2/−1 positions was previously noted (20, 21).

Endogenous GGA2 binds DXXLL signals better than does GGA1 or GGA3

We previously reported that full-length human GGA1 and GGA3 expressed in either insect or COS cells bound poorly to DXXLL motifs whereas GGA2 bound quite well to the same motifs (6). In contrast, the isolated VHS domains of all three GGAs bound equally well to the tested DXXLL peptides, indicating that other regions of GGA1 and GGA3 were inhibiting binding. We determined that this inhibitory activity was due to the presence of internal DXXLL sequences in the hinge regions of GGA1 and GGA3, while GGA2 lacks an internal DXXLL motif in the equivalent position. Mutation or deletion of these sequences released the inhibition (6).

These experiments utilized overexpressed proteins. To rule out the possibility that these proteins were altered in a manner that selectively impairs binding of GGA1 and GGA3 to DXXLL peptides, we tested the ability of endogenous human and mouse GGAs to bind DXXLL peptides in GST pull-down experiments. As shown in Figure 5, endogenous GGA2 from mouse brain and human HEK 293 cells bound very well to GST-CI-MPR peptide whereas endogenous GGA1 and GGA3 of both species exhibited undetectable or trace binding. Even the GST-CI-MPR peptide S→D mutant, which exhibits an increased affinity for GGA VHS domains (21), bound only weakly to endogenous GGA1 or GGA3, whereas

binding to GGA2 was strongly enhanced by the mutation. This difference in binding is not due to differences in affinities of the GGA1 and GGA3 VHS domains for the CI-MPR DXXLL signal compared to the GGA2 VHS domain. ITC measurements have shown that the *in vitro* binding constants of the isolated VHS domains of the three GGAs for the CI-MPR DXXLL peptide are very similar and lie in the 7–10 μM range (14, 17, 21). Taken together, these data suggest that endogenous GGAs 1 and 3 are in an inhibited state that impairs binding to the CI-MPR DXXLL peptide.

Alignment of GGA1 and GGA3 amino acid sequences across a number of mammalian species shows an internal AC-LL motif within the hinge region of all species examined (not shown). In contrast, the motif is absent in all orthologs of GGA2. Based on our pull-down experiments with mouse brain lysates, we postulated that the ^{354}SLLDDELM^{361} sequence within the mouse GGA1 hinge is responsible for the poor binding displayed by the endogenous protein. As shown in Figure 6A, wt mouse GGA1 binds poorly to the GST-CI-MPR peptide whereas a LM→AA mutation in the internal motif relieves this inhibition. As a control, both wt and mutant GGA1 bind equally well to a GST-fusion with the AP-1-γ appendage through the GGA1 hinge WNSF motif (22, 23). On the other hand, wt mouse GGA2 bound well under the same conditions, as did the isolated VHS domains of both GGA1 and GGA2 (Figure 6A, 6B). Truncation of GGA1 by introduction of a stop codon at amino acid 354 (which removes the DDELM sequence) but not at amino acid 369 relieved the inhibition, indicating that this internal DDELM sequence is the only motif responsible for inhibiting binding (Figure 6C). Furthermore, as reported for human GGA1, mutation of the upstream Ser 354 to Ala resulted in tighter binding to the GST-CI-MPR peptide whereas binding of the S→D mutant was inhibited to a greater extent than even the wt GGA1 (Figure 6D, long exposure). This effect was totally reversed by combining the S→D and LM→AA mutations (Figure 6E), showing that the former mutation does not disrupt the overall structure of the VHS domain but rather has a specific effect on binding to the internal motif peptide.

The internal DXXLL motif of LRP9 is sufficient to increase GGA1 localization at the TGN

A previous study (8) demonstrated that overexpression of wild-type (wt) LRP9 in COS cells increases recruitment of myc-GGA1 to the TGN. Moreover, the behavior of either the C-terminal or internal DXXLL motif mutant was indistinguishable from wt in terms of the increased TGN localization of GGA1, whereas mutation of both motifs resulted in decreased concentration of GGA1 at the TGN. The wt LRP9 construct used in that study had a C-terminal HA tag, effectively making both DXXLL motifs internal. Co-transfection of wt LRP9 containing a HA tag within the ectodomain of the protein with myc-GGA1 also increased localization of GGA1 at the TGN, as did the C-terminal DXXLL motif mutant of LRP9 (pLL/dLL→AA) (Figure 7). In the cells co-expressing GGA1 and wt or mutant LRP9, GGA1 was concentrated at the Golgi whereas this did not occur in the absence of LRP9 expression. This result shows that the internal motif of LRP9 is competent in recruiting GGA1 to the Golgi within a cell.

Discussion

We previously reported that GGA1 and GGA3 are subject to autoinhibition mediated by a DXXLL motif located in the hinge region of these coat proteins (6). Subsequently, we, and others identified a number of transmembrane proteins that harbor internal DXXLL motifs that interact with the GGAs (7–12, 24). As shown in Figure 1, most of these motifs are present within the C-terminal cytosolic tails of transmembrane proteins but in two instances are located within N-terminal cytoplasmic domains (11, 12). Furthermore, several reports show that the binding of C-terminal DXXLL motifs to GGAs is maintained upon addition of certain peptide tags to the C-termini of the corresponding proteins (8, 25, 26). In addition,

internal DXXLL motifs are sufficient for the recruitment of GGAs to the TGN membrane in Hela and COS cells as determined by immunoflourescence microscopy, indicating that internal motifs are functional GGA binding signals *in vivo* (8, 24, Figure 7). In contrast to these findings, Cramer *et al.* suggest that GGA binding is limited to DXXLL sites that are no more than 1-3 residues from the C-termini of cargo proteins and that GGA1 (and most likely GGA3) is not subject to autoinhibition mediated by an internal DXXLL motif (13).

We have now extended our initial studies of GGA binding to the internal DXXLL motifs of LRP9 and LRP12. Using the BLI system to measure peptide binding *in vitro*, we confirmed our previous findings based on GST pull-down assays that the internal DXXLL motif of LRP9 binds to GGA2 even though Cramer *et al.* reported that deletion of the C-terminal DXXLL signal of LRP9 abolished binding to the VHS domain of GGA1 (13). The fact that all the binding data with internal DXXLL motifs presented in our previous study (9) was performed with GGA2, while Cramer et al. (13) utilized only GGA1, raised the possibility that the discrepancy between the two studies relates to the use of alternate GGA adaptors, that is, GGA1 versus GGA2. However, we find little, if any, difference in the binding of internal DXXLL motifs to the three GGAs in GST pull-down assays (data not shown). In addition, as shown in Figure 7 (and reference 8), cells expressing LRP9 with the C-terminal DXXLL motif mutated recruit GGA1 onto the Golgi. The crystal structure of the GGA2 VHS domain does show a variance from that of GGA1/3 in that the loop between helices 6 and 7 of the GGA2 VHS ligand binding pocket undergoes a conformational change upon ligand binding (17). Thus, it was speculated whether such conformational flexibility would allow the GGA2 VHS domain to accommodate ligands of different peptide length (17). Hence, it will be interesting to see if more precise analysis of binding kinetics yields differences between GGA1 and GGA2 for internal DXXLL motifs.

Our modeling studies indicate that internal DXXLL motifs can dock in the binding groove of the VHS domains of the GGAs. This interaction is impacted by residues both upstream and downstream of the DXXLL sequence. The importance of acidic residues immediately upstream of the DXXLL motif has been documented previously (20, 21) and is confirmed by our finding that mutation of the residues in the −2/1 positions (Asp750 and Asp751 in LRP9) to Ala greatly diminished binding to GGA2. Mutation of the residues in the −4/−3 positions to Ala had only a minor effect on binding in the pull-down assay. Interestingly, our modeling shows that a relatively sharp turn near the N-termini of the DXXLL motifs is required to place the acidic residues at the −4/−3 positions in proximity to corresponding basic residues on the VHS domain surface (Figure 3). Such a strained conformation may counteract the binding energy gained by the formation of two additional salt bridges, resulting in relatively little net gain in affinity.

Importantly, mutation of the Pro at the +6 position also strongly impaired binding to the GGA2 VHS domain. Our modeling suggests that the proline interacts with the VHS domain surface. In addition, the proline also induces a bend in the peptide that may favor the simultaneous fitting of the DXXLL motif and the subsequent C-terminal residues into the binding groove of the VHS domain. Cramer *et al.* also suggested that a bend in the downstream segment of an internal DXXLL could allow binding in the groove, but concluded that this was unlikely to occur (13). In contrast, our modeling suggests that both bent and some unbent peptide conformations are readily accommodated by the VHS domain binding groove. These conformations place backbone polar groups and side-chains appropriately to interact with polar and hydrophobic groups near the C-termini of helices 6 and 8 of the VHS domain. Such interactions would compensate for the absence of interactions with a C-terminal carboxylate, making these conformations essentially isoenergetic with C-terminally located DXXLL motifs.

Thus, the nature of the amino acids surrounding the internal DXXLL motif strongly influence whether or not it interacts with the GGAs. Sometimes, these residues may even be in the −5/−4 position, as is the case with the CI-MPR DXXLL sequence, where simultaneous mutation of the two residues at the −5/−4 position completely abolished GGA binding in the yeast two-hybrid assay (20). A lack of appropriate residues surrounding the internal DXXLL motif of sorCS1 may explain why it does not bind GGAs (27) whereas the internal motifs of other proteins bind well. The importance of amino acids downstream of C-terminal DXXLL motifs has also been reported (14, 21, 28). These motifs are normally followed by 1-2 residues to the C-terminus, and the addition of 2–4 Ala to the CI-MPR signal (14, 28) or the addition of a Myc-tag to either Sortilin or the CI-MPR signal (13) prevents binding to the GGAs. However, the addition of different C-terminal tags to LERP, the *Drosophila melanogaster* homolog of the mammalian MPR, LRP9, and BACE does not prevent GGA binding (8, 9, 26). Taken together, these findings indicate that it is the specific sequence of the downstream residues rather than the number that determines the impact on binding to the GGAs.

Our previous studies of GGA1/3 autoinhibition utilized human proteins that were overexpressed in COS or insect cells (6). While mouse GGA1 and GGA3 are 91% and 85% identical in amino acid sequence to their human counterparts and share identical DXXLL motifs in their hinge segments, no actual GGA binding studies have been reported with the mouse GGAs. This afforded the opportunity to compare mouse GGA1/3 binding to DXXLL motifs with that of mouse GGA2 and to determine whether the former GGAs are subject to autoinhibition as occurs with human GGAs 1/3 in our GST pull-down assays. Our data clearly demonstrate that endogenous mouse GGA2 binds strongly to the CI-MPR DXXLL motif whereas binding of endogenous mouse GGA1 and GGA3 is extremely poor. A similar finding was reported by Stauber and Jentsch, who examined the interaction between the N-terminal DXXLL motif of the endosomal/lysosomal CLC chloride transporter, ClC7, and endogenous GGAs present in Hela cell lysates (12). Importantly, mutation of the internal DXXLL motif of mouse GGA1 greatly enhances binding. Furthermore, binding of the isolated GGA1-VHS domain to the DXXLL motif of the CI-MPR was equivalent to that observed with the VHS domain of GGA2. These findings replicate our results with human GGAs and support the conclusion that GGA1 and GGA3 are subject to autoinhibition mediated by binding of an internal DXXLL motif located in the hinge segment to the binding site of the VHS domain.

We note that there is an interesting and potentially important distinction between the internal GGA DXXLL motifs involved in intramolecular interactions and internal DXXLL motifs found in cargo receptors. The effective concentration of “tethered” motifs involved in *cis* interactions has been estimated to be in the range of 50 to 250 μM, depending on the length and flexibility of the linkers connecting the binding domain and the internal target binding motif (29). This is an order of magnitude higher than the dissociation constants measured for interactions between VHS domains and mimics of C-terminal DXXLL peptides *in vitro* (13, 14, 21). In order for cargo molecules to compete against autoinhibition, we would expect that either the effective binding affinity of the intrinsic GGA motifs for their own VHS domains should be relatively weak, and/or that this affinity is modulated by a switching mechanism such as phosphorylation. Our prior work has indeed shown that the latter mechanism occurs (6), and additional mechanisms such as changes in the overall conformation of the GGAs upon clathrin, ARF1 or ubiquitin binding may also be relevant. We therefore suggest that *in vitro* binding experiments to peptides mimicking the GGA internal DXXLL motifs would show correspondingly little binding and weak apparent affinities. Interestingly, the GGA internal motifs do not contain acidic residues upstream of the canonical aspartic acid (Figure 1). In addition, these motifs contain glycines at the position three residues C-terminal of the dileucine. These glycines would not pack

effectively against the K100 sidechain, but would allow for sufficient flexibility in the backbone to accommodate additional C-terminal residues without causing steric clashes with the VHS domain surface. The internal GGA motifs thus should bind intrinsically more weakly to the VHS domains and this would certainly be evident i*n trans*; however, the high effective concentration of these motifs *in cis* binding would allow them to form intramolecular contacts and place the GGA into an autoinhibited conformation.

In contrast, we would expect that the affinity of the GGA VHS domains for internal motifs located in cargo molecules such as LRP9 or LRP12 should be similar to those measured for C-terminal DXXLL motifs. Indeed, our BLI measurements suggest that this is the case, as we measure an affinity of 0.38±0.07μM for the interaction between GGA2 and the internal motif of LRP9 versus 0.12±0.03μM for the C-terminal motif of CI-MPR. Correspondingly, our modeling suggests that many or most of the canonical interactions observed for C-terminal DXXLL motifs are replicated when VHS domains bind to the internal motifs from LRP9 and LRP12. Moreover, our modeling shows that the internal placement of these motifs is very unlikely to produce steric conflicts and, in fact, allows for the formation of essentially as many productive contacts as would form upon binding of a C-terminally located DXXLL motif.

In conclusion, we believe that our data and that of other groups provide strong evidence that GGAs do bind some internal DXXLL motifs. We also conclude that both human and mouse GGA1 and GGA3 are subject to autoinhibition mediated by internal DXXLL motifs present in the hinge region of these proteins. The concept that GGAs are capable of binding internal DXXLL sequences has significant implications for understanding the role of GGAs in the trafficking of an array of cargo molecules and in the regulation of GGA1 and GGA3 action.

Materials and Methods

Materials

Mouse anti-HA monoclonal antibody was purchasedfrom Covance (Berkeley, CA), while the anti-HA rabbit polyclonal antibody was from Sigma (St. Louis, MO). The anti-myc 9E10 monoclonal antibody was from Santa Cruz Biotechnology, Inc. (Santa Cruz, CA), while the anti-Flag M2 monoclonal antibody was from Sigma (St. Louis, MO). For detection of endogenous GGAs, the following antibodies were used: anti-GGA1 (GGA1 H-215 for both mouse and human proteins) and anti-GGA2 (GGA2 H-175 for mouse protein) from Santa Cruz Biotechnology, Inc. (Santa Cruz, CA), anti-GGA2 (cat #612613 for human protein) and anti-GGA3 (cat#612311 for human protein) from BD Biosciences (Franklin Lakes, NJ), and anti-GGA3 made in-house against the purified VHS-GAT domain of recombinant mouse GGA3 to detect the protein of mouse origin. HRP-conjugated secondary antibodies, and Glutathione-Sepharose 4B were from GE Healthcare (Little Chalfont, Buckinghamshire, United Kingdom), while the Amylose Resin for purification of MBP and MBP fusion proteins was from New England BioLabs (Ipswich, MA). Lipofectamine Plus reagent for transfection was from Invitrogen (Carlsbad, CA) while proteinase inhibitors were from Roche Applied Science, (Indianapolis, IN). The strepavidin-coated Octet biosensor pins were purchased from ForteBio (Menlo Park, CA).

Computational modeling

LRP9 and LRP12 internal DXXLL motifs were docked against the crystal structure of the human GGA1 VHS domain using PDB entries 11JWF (apo-VHS domain) and 1JWG (complex of GGA1 VHS domain with C-terminal DXXLL motif peptide from the cation independent Mannose 6-phosphate receptor) as starting models. LRP9 was also docked against the crystal structure of the human GGA2 VHS domain (PDB entry 1MHQ (17),

superimposed onto the GGA1 VHS domain in 1JWG. Coot (30) was used to build initial docked models of the internal DXXLL motifs using the cation independent Mannose-6-phosphate receptor peptide as a template. As LRP9 contains two overlapping potential DXXLL motifs, the corresponding sequence was docked in two different positions on both GGA1 and GGA2, so that LRP9 residues 690 and 689 correspond to the canonical aspartic acid of the motif. Initial models were input into the FlexPepDock server (18, 19) for energy minimization, docking and model refinement. The only explicitly refined restraints included with the input files were the following: 1) Simple harmonic restraints between the canonical aspartic acid sidechain oxygens and the amide nitrogens of GGA1 F88 (2.6 Å ± 0.4 Å) and R89 (2.9Å ± 0.5 Å); 2) Simple harmonic restraint between the sidechain nitrogen of GGA1 N92 and the carbonyl oxygen of the residue preceding the first leucine (3.0Å ± 0.4 Å); 3) Simple harmonic restraint between the sidechain oxygen of GGA1 N92 and the amide nitrogen of the second leucine (2.9 Å ± 0.4 Å). 100 low- and 300 high-resolution models were generated and filtered in each docking procedure. The 10 best FlexPepDock models were saved and examined for common features and potential steric or geometric violations, of which none were observed. Output scores (Rosetta energies) ranged from −183 to −190 (GGA1 docking) or −237 to −241 (GGA2 docking) for the 10 best models for each docking procedure. Output models were examined and molecular graphics were generated using PyMol v.0.99 (31)

Plasmid construction

The plasmid encoding human Myc-GGA1 in the vector pCR3.1 has been described (6). The mouse LRP12, GGA1 and GGA2 clones encoding the complete cDNAs were obtained from American Type Culture Collection. The cDNAs were cloned into the vector pcDNA3.1 for expression in HEK 293 cells. A HA epitope was inserted immediately upstream of Glu-620 within the LRP12 cytosolic tail while N-terminal Flag-tags were appended to GGA1 and GGA2. Mutations were made using the QuikChange site-directed mutagenesis system (Agilent Technologies, Santa Clara, CA) and all constructs were sequenced prior to transfection. All LRP9 pLL→AA mutations entailed change of the three tandem leucines to alanines since the internal DXXLL sequence of LRP9 is effectively comprised of two overlapping motifs (see Figure 1). The LRP9 dLL→AA mutation changed the C-terminal DXXLL sequence to AXXAA. The GST-GGA2 VHS-GAT and GST-CI-MPR constructs have been described (4, 6).

Cell culture and transfection

Transient transfection of HEK 293 cells was achieved by transfectionof 4 μg plasmid DNA in 10 cm tissue culture dish according to the manufacture's instructions. Cells were harvested 48 h post-transfection and homogenized into phosphate-buffered saline containing 1% Triton X-100 (PBS-T) and proteinase inhibitors at 4°C. Untransfected 293 cells and mouse brain tissue were similarly processed and all homogenates were centrifuged at 15,000 × *g* for 15 min at 4°C, the supernatants were saved and the protein concentrations determined. Samples were diluted to 2 mg/ml in cold PBS-T for use in binding assays.

Immunofluorescence

Hela cells plated on coverslips were co-transfected with HA-LRP9 (wt or the dLL→AA mutant) (9) and myc-GGA1 (6), fixed 12 hr post-transfection with ice-cold 1:1 methanol-acetone solution for 5 mins, and processed for immunofluorescence microscopy as described (9). Cells were visualized using a ZEISS LSM 510 inverted confocal microscope with a Plan-Apo 63X/1.4 oil immersion objective (Carl Zeiss Microscopy, Thornwood, NY).

Expression/purification of GST and MBP fusion proteins

GST and MBP fusions in pGEX and pMal expression vectors, respectively, were expressed in the *Escherichiacoli* strain BL-21 (RIL) (Agilent Technologies, Santa Clara, CA). GST fusions were purified essentiallyas described previously (6). MBP and MBP fusions were eluted from the amylose resin with BLI buffer A (10 mM Hepes, pH 7.0, 150 mM NaCl, 3.4 mM EDTA, 0.05% Tween-20, and 20 mM maltose). Protein concentrations were determined prior to diluting eluted proteins with an equal volume of BLI buffer B (buffer A without maltose but with 2% BSA). All subsequent dilutions were performed with BLI buffer C (buffer A without maltose but with 1% BSA). This method ensured that the various concentrations of the different proteins were assayed under the same buffer conditions.

Pull-down assays

Pull-down assays were performed in a final volume of 300 μl in 1.5 ml pre-siliconized microcentrifuge tubes (MidSci, St. Louis, MO). Routinely, 100 μg GST-fusion proteins were first immobilized on 50 μl of packed glutathione-Sepharose 4B for 2 hours at room temperature. The beads with bound proteins were pelleted by centrifugation at 750 × *g* for 1 min, the beadswere washed once with PBS-T, and 300 μl of HEK 293 cell or mouse brain lysate in PBS-T at a final concentration of 2 mg/ml was added to the washed beads. The binding reactions were allowed to proceed for 2 h at 4°C with tumbling, after which the samples were subjected to centrifugation at 750 × *g* for 1min. An aliquot of the supernatant was saved, and the pellets were washed four times each by resuspension in 1 ml of cold PBS-T followed by centrifugation at 750 × *g*. The washed pellets were resuspendedin SDS sample buffer and heated at 100°C for 5 min, and pellet and supernatant fractions were resolved by SDS-PAGE, transferred to nitrocellulose membranes, and probed with anti-HA, anti-myc, or anti-Flag antibody. Nitrocellulose membranes were routinely stained with Ponceau solution to ascertain equal loadings of fusion proteins.

Direct binding using bio-layer interferometry (BLI)

Direct binding of DXXLL signals to mouse GGA2 was determined by BLI using a ForteBio Octet (Menlo Park, CA). Briefly, purified mouse Flag-GGA2 was subject to low-level biotinylation using a 1:1 molar ratio of GGA2 to EZ-Link NHS-PEG_4-Biotin (Thermo Scientific, Rockford, IL) at room temperature for 1 hr. The reactions were desalted on a Zeba Desalt Spin Column (Thermo Scientific, Rockford, IL) to remove free biotin and streptavidin-coated biosensors from ForteBio were used to capture the biotinylated GGA2 onto the surface of the sensor. After reaching base line, sensors were moved to the association step containing 5, 2.5, 1.25, 0.62, 0.31 and 0.15 μM MBP-peptides for 300 s and then dissociated for 300 s. A buffer-only (BLI buffer C) reference was subtracted from all curves. Affinities were estimated from global kinetic analysis of the five concentrations using Octet RED software version 5.2. R^2 (Table 1) is the square of the sample correlation coefficient between the outcomes and their predicted values.

Acknowledgments

We are very grateful to Eline van Meel for her assistance with confocal microscopy. This work was supported by the National Institutes of Health Grants CA08759 (to S.K.) and GM080271 (to S.M.).

References

1. Bonifacino JS. The GGA proteins: adaptors on the move. Nat Rev Mol Cell Biol. 2004; 5:23–32. [PubMed: 14708007]
2. Braulke T, Bonifacino JS. Sorting of lysosomal proteins. Biochim Biophys Acta. 2009; 1793:605–614. [PubMed: 19046998]

3. Puertollano R, Randazzo PA, Presley JF, Hartnell LM, Bonifacino JS. The GGAs promote ARF-dependent recruitment of clathrin to the TGN. Cell. 2001; 105:93–102. [PubMed: 11301005]
4. Zhu Y, Doray B, Poussu A, Lehto VP, Kornfeld S. Binding of GGA2 to the lysosomal enzyme sorting motif of the mannose 6-phosphate receptor. Science. 2001; 292:1716–1718. [PubMed: 11387476]
5. Bonifacino JS, Traub LM. Signals for sorting of transmembrane proteins to endosomes and lysosomes. Annu Rev Biochem. 2003; 72:395–447. [PubMed: 12651740]
6. Doray B, Bruns K, Ghosh P, Kornfeld S. Autoinhibition of the ligand-binding site of GGA1/3 VHS domains by an internal acidic cluster-dileucine motif. Proc Natl Acad Sci USA. 2002; 99:8072–8077. [PubMed: 12060753]
7. Kzhyshkowska J, Gratchev A, Martens JH, Pervushina O, Mamidi S, et al. Stabilin-1 localizes to endosomes and the trans-Golgi network in human macrophages and interacts with GGA adaptors. J Leukoc Biol. 2004; 76:1151–1161. [PubMed: 15345724]
8. Boucher R, Larkin H, Brodeur J, Gagnon H, Thériault C, et al. Intracellular trafficking of LRP9 is dependent on two acidic cluster/dileucine motifs. Histochem Cell Biol. 2008; 130:315–327. [PubMed: 18461348]
9. Doray B, Knisely JM, Wartman L, Bu G, Kornfeld S. Identification of acidic dileucine signals in LRP9 that interact with both GGAs and AP-1/AP-2. Traffic. 2008; 9:1551–1562. [PubMed: 18627575]
10. Zhang J, Gratchev A, Riabov V, Mamidi S, Schmuttermaier C, et al. A novel GGA-binding site is required for intracellular sorting mediated by stabilin-1. Mol Cell Biol. 2009; 29:6097–105. [PubMed: 19752197]
11. del Castillo FJ, Cohen-Salmon M, Charollais A, Caille D, Lampe PD, et al. Consortin, a trans-Golgi network cargo receptor for the plasma membrane targeting and recycling of connexins. Hum Mol Genet. 2010; 19:262–275. [PubMed: 19864490]
12. Stauber T, Jentsch TJ. Sorting motifs of the endosomal/lysosomal CLC chloride transporters. J Biol Chem. 2010; 285:34537–34548. [PubMed: 20817731]
13. Cramer JF, Gustafsen C, Behrens MA, Oliveira CL, Pedersen JS, Madsen P, Petersen CM, Thirup SS. GGA autoinhibition revisited. Traffic. 2010; 11:259–73. [PubMed: 20015111]
14. Misra S, Puertollano R, Kato Y, Bonifacino JS, Hurley JH. Structural basis for acidic-cluster-dileucine sorting-signal recognition by VHS domains. Nature. 2002; 415:933–937. [PubMed: 11859375]
15. Shiba T, Kametaka S, Kawasaki M, Shibata M, Waguri S, Uchiyama Y, Wakatsuki S. Insights into the phosphoregulation of beta-secretase sorting signal by the VHS domain of GGA1. Traffic. 2004; 5:437–448. [PubMed: 15117318]
16. Shiba T, Takatsu H, Nogi T, Matsugaki N, Kawasaki M, Igarashi N, Suzuki M, Kato R, Earnest T, Nakayama K, Wakatsuki S. Structural basis for recognition of acidic-cluster dileucine sequence by GGA1. Nature. 2002; 415:937–941. [PubMed: 11859376]
17. Zhu G, He X, Zhai P, Terzyan S, Tang J, Zhang XC. Crystal structure of GGA2 VHS domain and its implication in plasticity in the ligand binding pocket. FEBS Lett. 2003; 537:171–176. [PubMed: 12606052]
18. Raveh B, London N, Schueler-Furman O. Sub-angstrom modeling of complexes between flexible peptides and globular proteins. Proteins. 2010; 78:2029–2040. [PubMed: 20455260]
19. London N, Raveh B, Cohen E, Fathi G, Schueler-Furman O. Rosetta FlexPepDock web server--high resolution modeling of peptide-protein interactions. Nucleic Acids Res. 2011; 39:W249–253. [PubMed: 21622962]
20. Puertollano R, Aguilar RC, Gorshkova I, Crouch RJ, Bonifacino JS. Sorting of mannose 6-phosphate receptors mediated by the GGAs. Science. 2001; 292:1712–1716. [PubMed: 11387475]
21. Kato Y, Misra S, Puertollano R, Hurley JH, Bonifacino JS. Phosphoregulation of sorting signal-VHS domain interactions by a direct electrostatic mechanism. Nat Struct Biol. 2002; 9:532–536. [PubMed: 12032548]
22. Inoue M, Shiba T, Ihara K, Yamada Y, Hirano S, Kamikubo H, Kataoka M, Kawasaki M, Kato R, Nakayama K, Wakatsuki S. Molecular basis for autoregulatory interaction between GAE domain and hinge region of GGA1. Traffic. 2007; 8:904–913. [PubMed: 17506864]

23. Bai H, Doray B, Kornfeld S. GGA1 interacts with the adaptor protein AP-1 through a WNSF sequence in its hinge region. J Biol Chem. 2004; 279:17411–17417. [PubMed: 14973137]
24. Hirst J, Carmichael J. A potential role for the clathrin adaptor GGA in Drosophila spermatogenesis. BMC Cell Biol. 2011; 12:22. [PubMed: 21599933]
25. Dennes A, Cromme C, Suresh K, Kumar NS, Eble JA, Hahnenkamp A, Pohlmann R. The novel Drosophila lysosomal enzyme receptor protein mediates lysosomal sorting in mammalian cells and binds mammalian and Drosophila GGA adaptors. J Biol Chem. 2005; 280:12849–12857. [PubMed: 15664992]
26. von Arnim CA, Tangredi MM, Peltan ID, Lee BM, Irizarry MC, Kinoshita A, Hyman BT. Demonstration of BACE (beta-secretase) phosphorylation and its interaction with GGA1 in cells by fluorescence-lifetime imaging microscopy. J Cell Sci. 2004; 117:5437–5445. [PubMed: 15466887]
27. Hermey G, Keat SJ, Madsen P, Jacobsen C, Petersen CM, Gliemann J. Characterization of sorCS1, an alternatively spliced receptor with completely different cytoplasmic domains that mediate different trafficking in cells. J Biol Chem. 2003; 278:7390–7396. [PubMed: 12482870]
28. Doray B, Bruns K, Ghosh P, Kornfeld S. Interaction of the cation-dependent mannose 6-phosphate receptor with GGA proteins. J Biol Chem. 2002; 277:18477–18482. [PubMed: 11886874]
29. van Valen D, Haataja M, Phillips R. Biochemistry on a leash: the roles of tether length and geometry in signal integration proteins. Biophys J. 2009; 96:1275–1292. [PubMed: 19217847]
30. Emsley P, Lohkamp B, Scott WG, Cowtan K. Features and development of Coot. Acta Crystallogr D Biol Crystallogr. 2010; 66:486–501. [PubMed: 20383002]
31. DeLano, WL. The PyMOL molecular graphics system. 2002. http://pymol.sourceforge.net

Figure 1. Sequence alignment of a number of internal DXXLL motifs

The numbers on the right indicate the C-termini of the proteins. ClC7 is a multi-pass transmembrane protein while consortin is a type-II membrane protein. (h=human, m=mouse, d=drosophila). Residues mutated in this study are shown in bold.

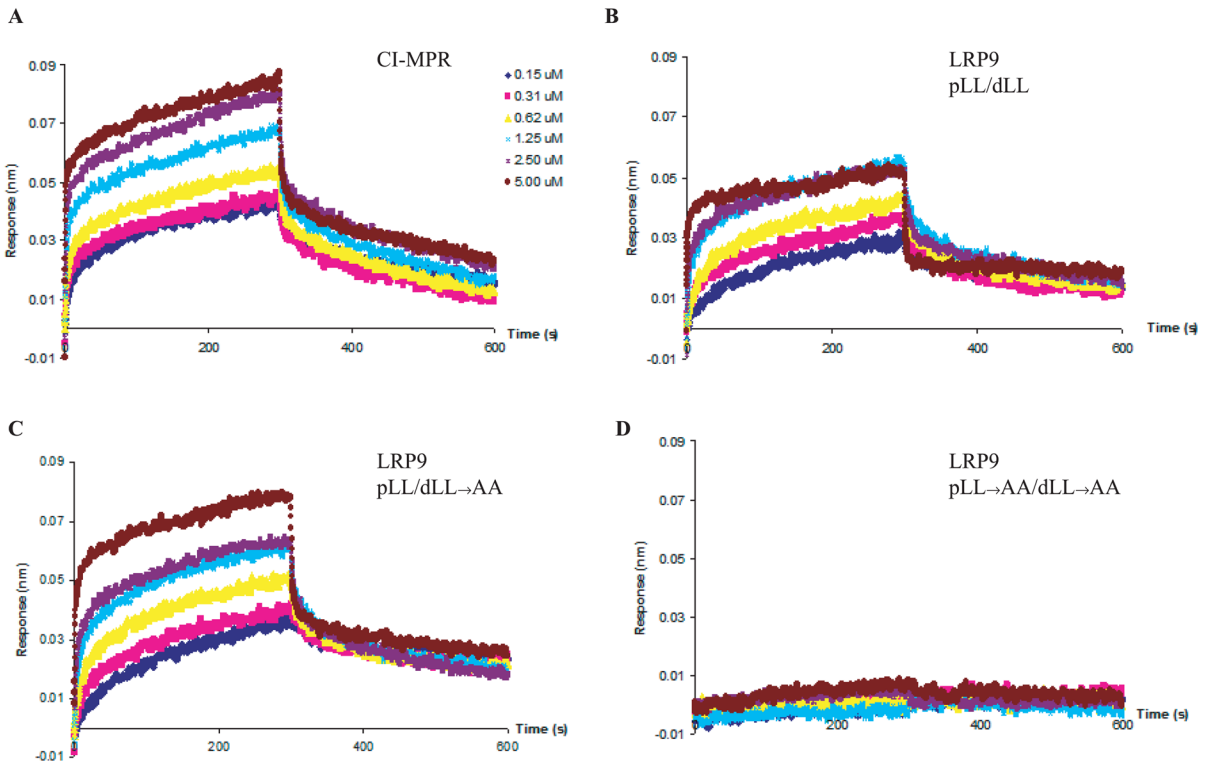

Figure 2. GGA2-DXXLL peptide binding assay

Biolayer interferometry was used to assay the binding of various DXXLL peptides to purified GGA2 (A–D). The association and dissociation of increasing concentrations of the different MBP-peptides to GGA2 are shown (A–D). The affinity (Table 1) of the peptides for GGA2 was calculated after subtraction of the signals obtained with MBP alone. The sequences of the ligands are as follows: CI-MPR – DDS**D**ED**LL**HV; LRP9 pLL/dLL – EDE**DD**V**LLL**……EAE**D**EP**LL**A; pLL/dLL→AA–EDE**DD**V**LLL** …….EAE**A**EP**AA**A; pLL→AA/dLL→AA–EDE**DD**V**AAA**…..EAE**A**EP**AA**A

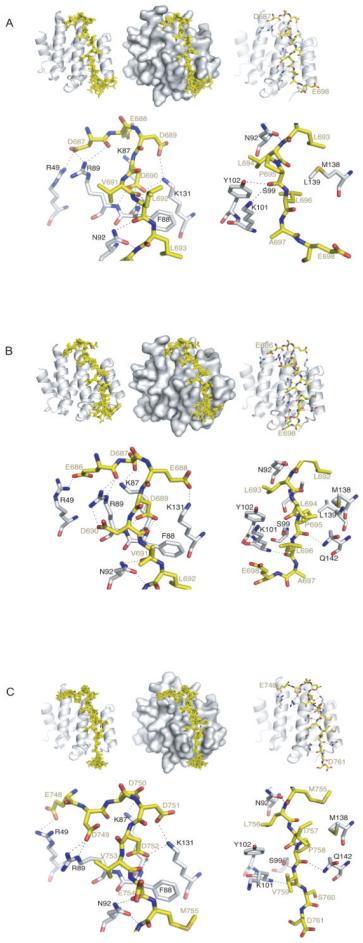

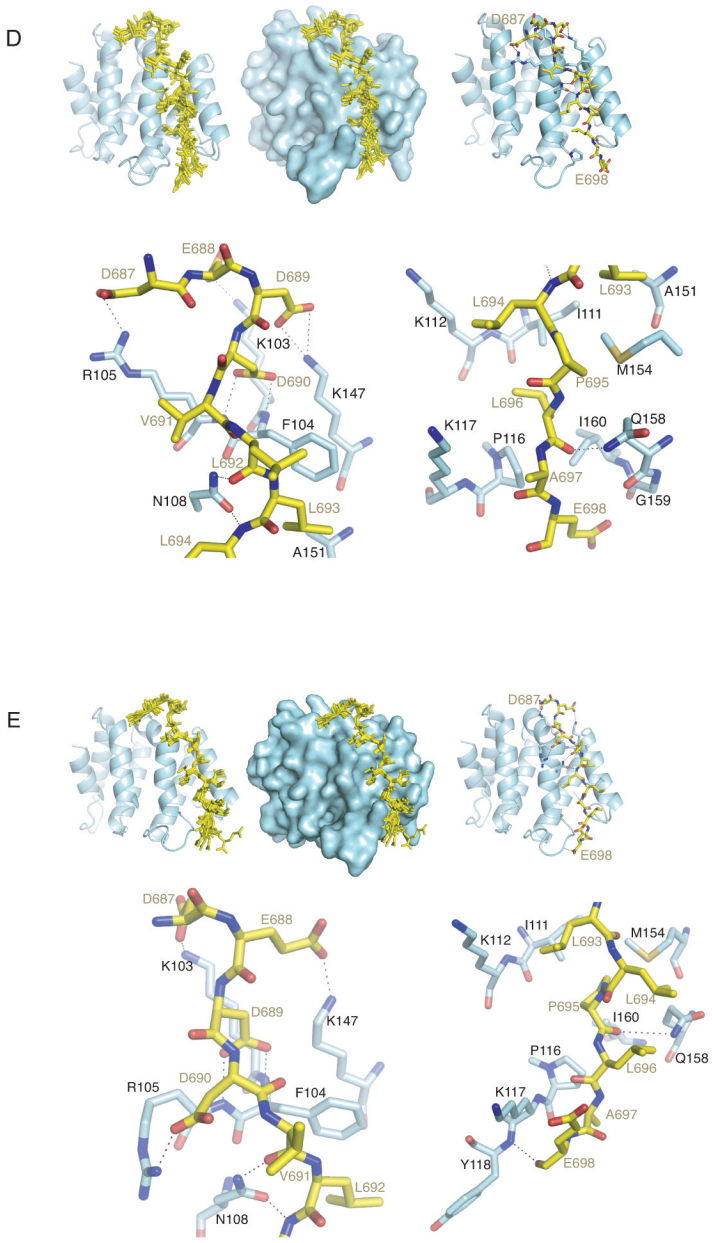

Figure 3. Modeling of complexes between the LRP9 and LRP12 internal DXXLL motifs with the GGA1-VHS domain

Computational docking of the LRP9 and LRP12 internal DXXLL motifs to the VHS domain of human GGA1 or GGA2 (See Materials and Methods for details). As LRP9 contains two overlapping potential DXXLL motifs, the corresponding sequence was docked in two different positions so that LRP9 residues 690 and 689 correspond to the canonical aspartic acid of the motif respectively (panels A and B). Panel (C) shows the docking of the LRP12 DXXLL motif. Panels (D) and (E) show the docking of the LRP9 motif to the GGA2 VHS domain in the same registers as in panels (A) and (B), respectively. In each panel, the upper row shows the conformations of the 10 best models from FlexPepDock (yellow stick representation) docked onto the VHS domain in white (GGA1) or light blue (GGA2) cartoon and surface representations. The rightmost structure in the top row shows the best-scoring

peptide model. The bottom row shows closeup views of respectively, 1) the canonical aspartic acid and surrounding residues; and 2) the dileucine motif and additional C-terminal residues. LRP9 and LRP12 residues are shown in stick representation with yellow carbon atoms, GGA1 VHS domain residues are shown with white carbon atoms, and GGA2 VHS domain residues are shown with light blue carbon atoms. Dotted lines indicated putative hydrogen bonds or salt bridges.

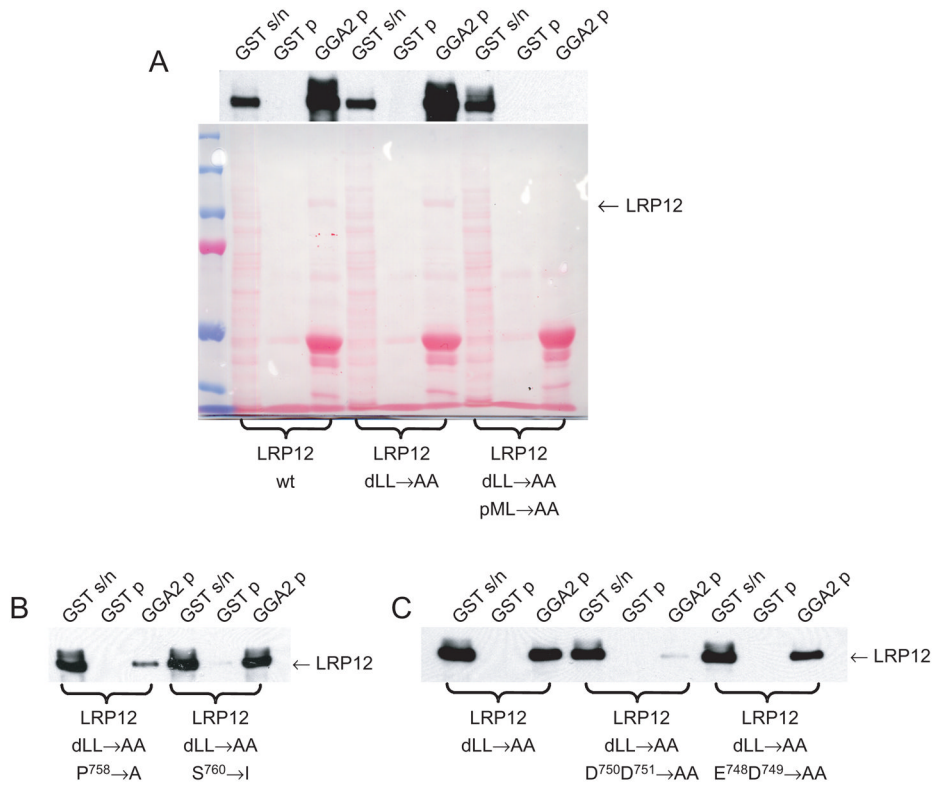

Figure 4. Residues outside of the core internal DXXLL motif significantly impact binding

(A–C) Pull down assays were performed using either GST or the GST-GGA2 VHS-GAT domain with HEK 293 cell-expressed wild-type (wt) and mutant LRP12 encoding a HA epitope at position 620 within the cytoplasmic tail. 2% of the supernatant (s/n) and 10% of the pellet (p) fractions were loaded for immunoblot analysis (AC) while 2% of the supernatant and 30% of the pellet fractions were loaded for Ponceau Red visualization of the LRP12 band in the affinity pull-down with GGA2 (A-lower panel). Membrane blots were probed with an anti-HA antibody (A–C).

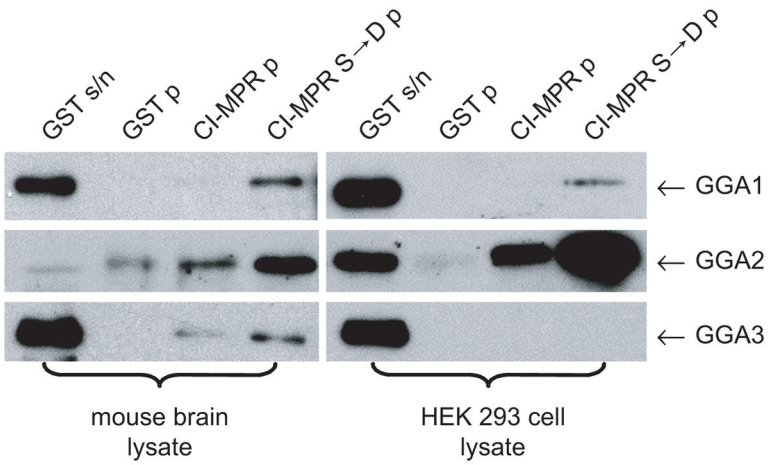

Figure 5. Endogenous GGA2 binds well to the CI-MPR DXXLL signal but not endogenous GGA1 or GGA3

Pull down assays were performed using either GST or the GST-CI-MPR DXXLL peptide with mouse brain cytosol or untransfected HEK 293 cell lysate. A single binding reaction was performed for the control protein (GST) and the ligand peptide (CI-MPR) using the two different lysates as a source of endogenous GGAs. Each pellet fraction was divided into 3 equal parts for SDS-PAGE and Western blot analysis and individually probed for GGA1, GGA2 and GGA3 as described under Materials & Methods. 5% of the GST supernatant was loaded to indicate input.

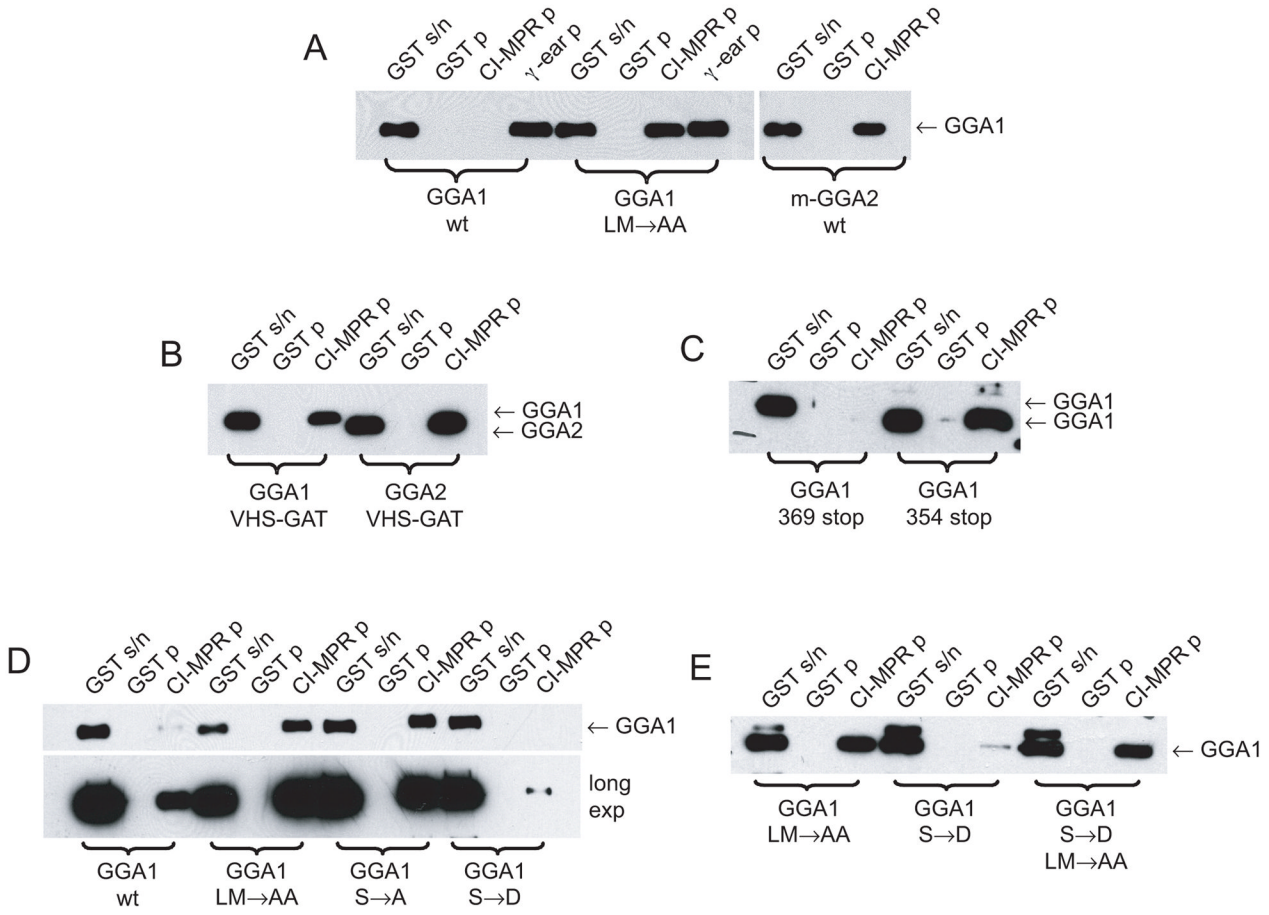

Figure 6. Mouse GGA1 is autoinhibited similar to its human ortholog

(A–E) Pull down assays were performed using either GST or the GST-CI-MPR DXXLL peptide with HEK 293 cell-expressed wild-type (wt) or mutant mouse GGA1-Flag. All GGA1 proteins are full-length unless otherwise indicated. GGA1 VHS-GAT encodes the first 332 and GGA2 VHS-GAT encodes the first 325 amino acids of their respective full-length proteins. The amino acids mutated within the GGA1 hinge are shown in bold in Figure 1. GST-AP-1 γ-ear was included as a positive control in A. 2% of the supernatant (s/n) and 10% of the pellet (p) fractions were loaded for SDS-PAGE and Western blotting (A–E). The blots were probed with an anti-Flag antibody to detect the wt and mutant GGA1.

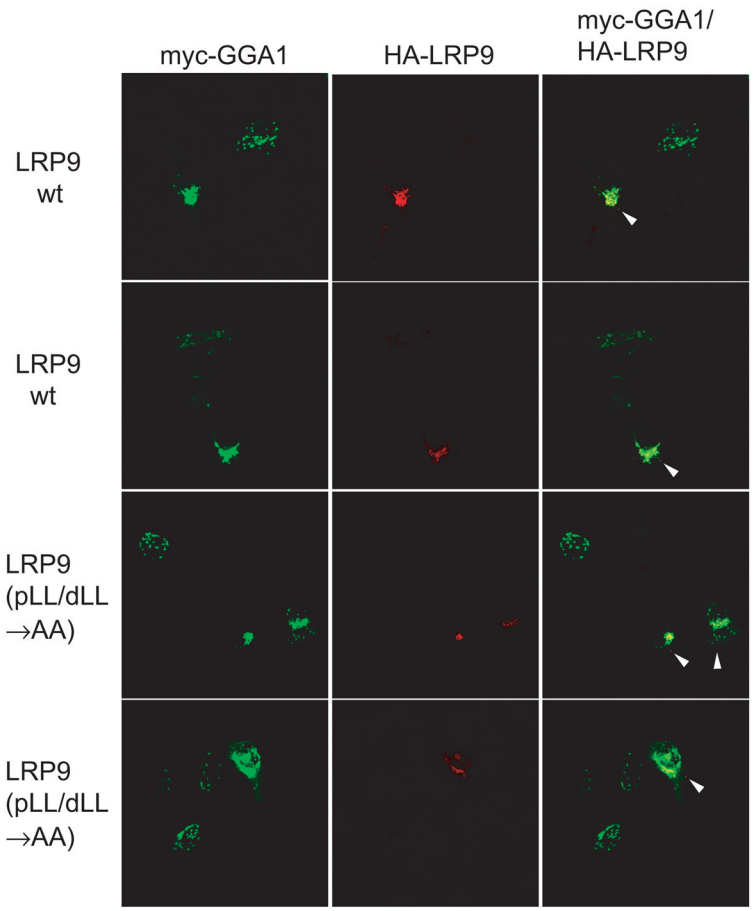

Figure 7. The internal DXXLL motif of LRP9 recruits GGA1 to the TGN

Hela cells co-transfected with myc-GGA1, and either wt HA-LRP9 (top two panels) or the C-terminal DXXLL mutant (pLL/dLL→AA) (bottom two panels), were probed with an anti-myc mouse monoclonal antibody or an anti-HA rabbit polyclonal antibody as described in Materials and Methods. Only cells co-expressing GGA1 and LRP9 (wt and mutant) show enhanced Golgi localization of the GGA (*arrowheads*).

Table 1

Binding constants for DXXLL peptide interactions with GGA2

MBP*-Peptides	Kd (μM)	k_{on} (1/Ms)	k_{off} (1/s)	R^2
CIMPR	0.12±0.04	3.8±1.6E4	4.2±0.9E-3	0.89±0.02
pLL/dLL	0.15±0.04	4.0±0.2E4	5.2±1.2E-3	0.87±0.01
pLL/dLL→AA	0.28±0.08	2.0±0.8E4	5.9±2.0E-3	0.87±0.03
pLL→AA/dLL→AA	NB**	NB**	NB**	NB**

*MBP=Maltose Binding Protein

**NB=No detectable binding